

# Halogen Bonding Propensity in Solution: Direct Observation and Computational Prediction

Taylor A. Bramlett<sup>[a]</sup> and Adam J. Matzger<sup>\*[a, b]</sup>

**Abstract:** Halogen-bonded complexes are often designed by consideration of electrostatic potential (ESP) predictions. ESP predictions do not capture the myriad variables associated with halogen bond (XB) donors and acceptors; thus, binding interaction cannot be quantitatively predicted. Here, a discrepancy between predictions based on ESP energy difference ( $\Delta V_s$ ) and computed gas phase binding energy ( $\Delta E_{\text{bind}}$ ) motivated the experimental determination of the relative strength of halogen bonding interactions in solution by Raman spectroscopic observation of complexes formed from

interacting five iodobenzene-derived XB donors and four pyridine XB acceptors. Evaluation of  $\Delta E_{\text{bind}}$  coupled with absolutely-localized molecular orbital energy decomposition analysis (ALMO-EDA) deconvolutes halogen bonding energy contributions and reveals a prominent role for charge transfer (CT) interactions. Raman spectra reveal  $\Delta E_{\text{bind}}$  accurately predicts stronger interactions within iodopentafluorobenzene (IPFB) complexes than with 1-iodo-3,5-dinitrobenzene (IDNB) complexes even though IPFB has similar electrostatics to IDNB and contains a smaller  $\sigma$ -hole.

## Introduction


The implementation of non-covalent interactions, such as hydrogen bonding, into supramolecular complex design in chemistry and biology is an attractive approach for molecular recognition.<sup>[1–3]</sup> Toward this pursuit, various avenues are being investigated to establish robust strategies that can encompass a wide variety of molecular design processes. Halogen bonding, a directional non-covalent interaction between a halogen atom (X) and a Lewis base (LB),<sup>[4–7]</sup> has been observed to facilitate strong and directional interactions in the solid state, solution, and gas phase and is well described with computational modeling.<sup>[8]</sup> Formation of these types of interactions is associated with a  $\sigma$ -hole,<sup>[6,9,10]</sup> a region of electropositive potential located on the halogen atom along the axis of the covalent bond, that allows halogens to act as electron pair acceptors upon interaction with a LB.<sup>[9]</sup> The strength of halogen bonding interactions and extent to which the  $\sigma$ -hole magnitude increases relate to the polarizability of halogen atoms following the order of  $F < Cl < Br < I$ .<sup>[7]</sup> Iodine, the most polarizable in the series, develops larger  $\sigma$ -holes which can lead to stronger interactions upon complexation.<sup>[11,12]</sup>

Since the discovery of halogen bonding, researchers have been exploring the ways in which halogen bonds (XBs) are affected by substituents in both aromatic<sup>[13]</sup> and non-aromatic systems; designing halogen bond donor/acceptor complexes and employing computational methods that can predict halogen bonding interactions and their strengths remains an active area of research.<sup>[4,14]</sup> Commonly evaluated concepts pertaining to the driving forces for halogen bonding interactions are polarizability, dispersion, charge transfer, and electrostatics, which are accessible from computational methods.<sup>[15]</sup> Design strategies for non-covalent complex formation frequently utilize electrostatic potential (ESP)<sup>[16–18]</sup> maps of both the donor and acceptor as a way to predict interaction propensities thus enabling correlations to interaction strengths to be made.<sup>[16,19]</sup> ESP maps are used as quantitative representations of charge distribution characterized by maximum electrostatic potential ( $V_{s,\text{max}}$ ) and minimum electrostatic potential ( $V_{s,\text{min}}$ ) values;<sup>[16,20,21]</sup>  $V_{s,\text{max}}$  and  $V_{s,\text{min}}$  are relevant to the magnitude of the  $\sigma$ -hole and lone pairs, respectively.

Many studies have reported taking advantage of ESP maps as a predictive tool for the design of solid-state supramolecular assemblies.<sup>[16–19,22,23]</sup> In cases involving halogen bonding between aromatic partners,<sup>[23,24]</sup> the approach for selecting XB donors and acceptors relies on electron withdrawing or donating substituents that activate the interacting sites involved.<sup>[18,22,24]</sup> The best donors contain large positive  $V_{s,\text{max}}$  values and the best acceptors have large negative  $V_{s,\text{min}}$  values. Though the use of ESP maps to predict interactions in the solid state is common,<sup>[16,25]</sup> such interactions are perturbed by competition among hierarchies of intermolecular forces<sup>[24]</sup> that facilitate assembly within a crystal lattice making direct correlations tenuous. To overcome this challenge, we have set out to investigate solution phase halogen bonding to evaluate the use of theoretical gas phase binding energies ( $\Delta E_{\text{bind}}$ )<sup>[26]</sup> to predict favorable halogen bonding propensities.<sup>[27–29]</sup>  $\Delta E_{\text{bind}}$  are

[a] T. A. Bramlett, Prof. Dr. A. J. Matzger  
Department of Chemistry  
University of Michigan  
930 North University Ave, Ann Arbor MI 48109 (USA)  
E-mail: matzger@umich.edu

[b] Prof. Dr. A. J. Matzger  
Macromolecular Science and Engineering Program  
Department of Chemistry  
University of Michigan  
930 North University Ave, Ann Arbor MI 48109 (USA)

 Supporting information for this article is available on the WWW under <https://doi.org/10.1002/chem.202102522>

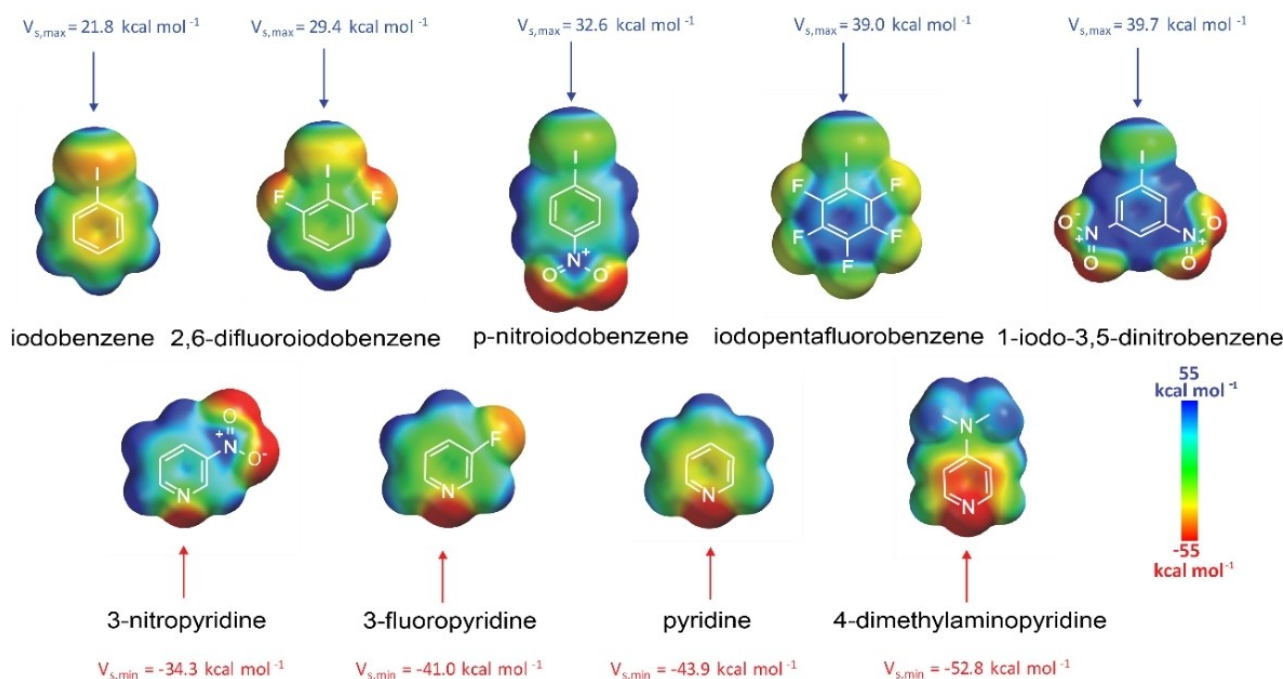


**Figure 1.** ESP maps of iodinated halogen bond donors and pyridine derived acceptors to visualize  $V_{s,max}$  (blue) and  $V_{s,min}$  (red) regions in  $\text{kcal mol}^{-1}$  at the B3LYP/6-311G\*\* level of theory.

then compared with predictions from ESP maps, as a predictor of halogen bonding propensities in solution. Five iodinated XB donors with various extents of electronic activation and four nitrogen heterocyclic XB acceptors are experimentally assessed via Raman spectroscopy to analyze interaction propensity.

## Results and Discussion

### Electronic effects on XB strength

ESP maps were used to choose complementary XB donor and acceptor pairs in Figure 1. The values associated with the most positive and negative electrostatic potentials, on the ESP maps (0.002 e/au isosurface) for a given XB donor and acceptor, are  $V_{s,max}$  and  $V_{s,min}$ , respectively.<sup>[20]</sup> Electron withdrawing substituents (fluoro and nitro) influence the strength of XB donors through the activation of the  $\sigma$ -hole.<sup>[27,28,30]</sup> The  $\sigma$ -hole magnitude of the iodobenzenes increases in the order iodobenzene (IB) < 2,6-difluoriodobenzene (DFIB) < p-nitroiodobenzene (p-NIB), < iodopentafluorobenzene (IPFB) < 1-iodo-3,5-dinitrobenzene (IDNB).  $V_{s,max}$  values range between positive ESPs of  $21.8 \text{ kcal mol}^{-1}$ , for the smallest  $\sigma$ -hole containing molecule (IB), and  $39.7 \text{ kcal mol}^{-1}$  for the largest (IDNB).  $V_{s,min}$  values for the XB acceptors increase as acceptor strengths of the nitrogen atom lone pairs increase. XB acceptor strengths increase following the trend: 3-nitropyridine (3-NPy) < 3-fluoropyridine (3-FPy) < pyridine (PY) < 4-dimethylaminopyridine (DMAP). Negative  $V_{s,min}$  values ( $-34.3 \text{ kcal mol}^{-1}$  for the weakest acceptor 3-NPy) to  $-52.8 \text{ kcal mol}^{-1}$  (for the strongest acceptor DMAP) are calcu-

lated. Table 1 lists all XB donors and acceptors with corresponding  $V_{s,max}$  and  $V_{s,min}$  values.

The  $V_{s,min}$  value from an interacting acceptor was subtracted from the  $V_{s,max}$  value from a donor to produce an electrostatic potential energy difference value ( $\Delta V_s$ ). It has been hypothesized that the energy difference ( $\Delta V_s = V_{s,max} - V_{s,min}$ ) between a donor and acceptor pair suggests how strongly a donor would interact with an acceptor.<sup>[16]</sup> Table 2 shows that when the difference between  $V_{s,max}$  and  $V_{s,min}$  of all XB donors and acceptors is applied, the  $\Delta V_s$  values of the 20 complexes suggest an increase in halogen bonding propensities as  $\Delta V_s$

**Table 1.** Electrostatic potential values for the XB donors and acceptors in  $\text{kcal mol}^{-1}$  calculated at B3LYP/6-311G\*\* level.

XB Donors	$V_{s,max}$	XB Acceptor	$V_{s,min}$
IB	21.8	3-NPy	-34.3
DFIB	29.4	3-FPy	-41.0
p-NIB	32.6	PY	-43.9
IPFB	39.0	DMAP	-52.8
IDNB	39.7		

**Table 2.**  $\Delta V_s$  values of all 20-halogen bond donor/acceptor complexes in  $\text{kcal mol}^{-1}$  calculated at B3LYP/6-311G\*\* level.

XB Acceptors	XB Donors				
	IB	DFIB	p-NIB	IPFB	IDNB
3-NPy	56.1	63.7	66.9	73.3	74.0
3-FPy	62.8	70.4	73.6	80.0	80.7
PY	65.7	73.3	76.5	82.9	83.6
DMAP	74.6	82.2	85.4	91.8	92.5

increases positively from 56.1 kcal mol<sup>-1</sup> for IB/3-NPy to 92.5 kcal mol<sup>-1</sup> for IDNB/DMAP. IDNB is the largest  $\sigma$ -hole containing XB donor of the series with the greatest  $\Delta V_s$  energy difference and is predicted, based on the  $\Delta V_s$  values, to have the strongest interactions with all the acceptors. Note, IPFB follows closely behind IDNB having  $\Delta V_s$  energy difference values between donor and acceptor pairs less than 1 kcal mol<sup>-1</sup> weaker.

Though ESPs have been demonstrated as a way to predict bonding preferences,<sup>[17,22,27]</sup> there are a multitude of energy factors aside from electrostatics<sup>[31]</sup> that influence binding affinities of XB donor/acceptor pairs that are not taken into account.<sup>[32,33]</sup> As a means of considering the energy factors that contribute to halogen bonding interactions as a whole, theoretical binding energy ( $\Delta E_{\text{bind}} = E_{\text{complex}} - (E_{\text{XB donor}} + E_{\text{XB acceptor}})$ ), which encompasses the total energy of each XB donor, acceptor, and complex, was explored (Table S1 in Supporting Information for listing of total energies). Calculated  $\Delta E_{\text{bind}}$  values for the selected XB donor/acceptor complexes are shown in Table 3.

Application of  $\Delta E_{\text{bind}}$  to the halogen bonded donor/acceptor complexes led to the evaluation of halogen bonding interaction trends affected not only by electrostatics, but also additional energy terms.  $\Delta E_{\text{bind}}$  values were plotted against XB acceptor strengths, represented by  $V_{s,\text{min}}$  values, and a linear correlation was found (Figure 2) suggesting that binding energies for a given halogen bond donor/acceptor complex are well predicted by acceptor strength. By contrast donor strengths correlate to binding energies but are considerably weaker than the acceptor strengths (Figure S3 in Supporting Information). Figure 2 illustrates that as negative  $V_{s,\text{min}}$  values increase following the trend 3-NPy < 3-FPy < PY < DMAP, there is an increase in the negative  $\Delta E_{\text{bind}}$  values (i.e. binding affinity) within the XB donor/acceptor

complexes. DMAP, with a  $V_{s,\text{min}} = -52.8$  kcal mol<sup>-1</sup>, is a better XB acceptor for all XB donors than PY ( $V_{s,\text{min}} = -43.9$  kcal mol<sup>-1</sup>), which out-competes 3-FPy ( $V_{s,\text{min}} = -41.0$  kcal mol<sup>-1</sup>) and 3-NPy ( $V_{s,\text{min}} = -34.3$  kcal mol<sup>-1</sup>), and thus forms the strongest XB donors/acceptor complexes.

With respect to the chosen basis set, the B3LYP functional can underestimate forces contributing to association<sup>[34]</sup> thus a D3 dispersion correction was also examined (see Table S2 in Supporting Information). B3LYP-D3 calculations show that while the trends in binding energies are the same as B3LYP, the binding energies of the complexes are more attractive in nature (average = 2.58 ± 0.26 kcal mol<sup>-1</sup>) with shorter interaction distances (average = 0.04 ± 0.02 Å) than in B3LYP (Table S4 in Supporting Information). Additionally,  $\Delta E_{\text{bind}}$  calculations were undertaken in the solvent model dichloromethane (DCM) to compare interaction stability. For the DCM solvent model (Table S3), all XB donor/acceptor complexes are found to have binding energies that are less attractive (average = 1.17 ± 0.56 kcal mol<sup>-1</sup>) though with shorter interaction distances (average = 0.05 ± 0.03 Å) than those shown in the Table 3 (S4 in Supporting Information). The tendency for halogen bonded complexes to have shorter interaction distances in solvent models has been previously reported.<sup>[35]</sup>

$\Delta E_{\text{bind}}$  is a property assigned to a halogen bonding complex and not just the single XB donor or acceptor molecules and therefore consideration was given to the electrostatic potential equivalent,  $\Delta V_s$ , for insight into predicting halogen bonding interaction trends. When  $\Delta E_{\text{bind}}$  values were plotted against  $\Delta V_s$  values (Figure 3), an increase in the strength of the XB donor results in steeper slopes ( $m$ ) denoting favorable complexation (e.g., IB/acceptor complex ( $m = -0.080$ ) < DFIB/acceptor complex ( $m = -0.116$ ) < p-NIB/acceptor complex ( $m = -0.134$ ) < IDNB/acceptor complex ( $m = -0.192$ ) < IPFB/acceptor complex ( $m = -0.194$ )). The parallel slopes of DFIB and p-NIB/acceptor complexes as well as IDNB and IPFB/acceptor complexes reflect a similar sensitivity within the pairs toward XB acceptors. However, the different slopes evident in Figure 3 suggest that there are energy terms in  $\Delta E_{\text{bind}}$  missing from  $\Delta V_s$  predictions that differentially affect the complexes containing fluorinated and nitrated XB donors.

ESP predictions, specifically for IPFB and IDNB/acceptor complexes, show that electrostatics alone do not fully describe

**Table 3.** Theoretical binding energies ( $\Delta E_{\text{bind}}$ ) of all XB donor/acceptor complexes in kcal mol<sup>-1</sup> calculated at B3LYP/6-311G\*\* level.

XB Acceptors	XB Donors				
	IB	DFIB	p-NIB	IPFB	IDNB
3-NPy	-2.53	-4.16	-3.48	-5.26	-4.37
3-FPy	-2.95	-4.73	-4.26	-6.20	-5.34
PY	-3.31	-5.17	-4.81	-7.00	-6.09
DMAP	-3.97	-6.27	-5.93	-8.77	-7.86

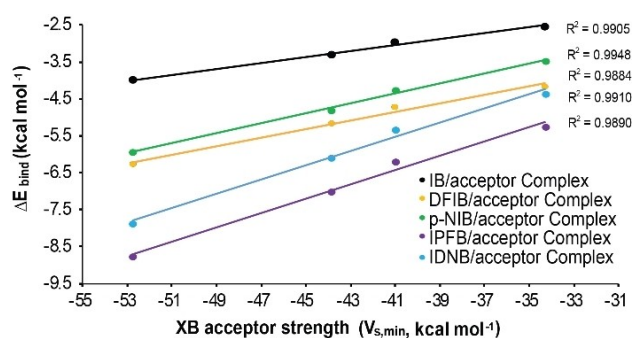


**Figure 2.** Graph representing the correlation between  $\Delta E_{\text{bind}}$  and XB acceptor strength ( $V_{s,\text{min}}$  kcal mol<sup>-1</sup>).

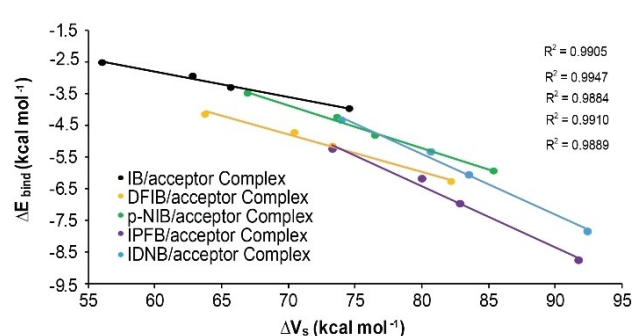


**Figure 3.** Graph representing the correlation between  $\Delta E_{\text{bind}}$  and  $\Delta V_s$  in kcal mol<sup>-1</sup>.

binding energy trends thus motivating a more thorough analysis of unaccounted for energy terms that can be derived by deconvoluting total energy. The total intermolecular interaction energies for the IPFB/acceptor complexes and IDNB/acceptor complexes were partitioned by absolutely-localized molecular orbital energy decomposition analysis (ALMO-EDA) using the Q-Chem 5.3.2 software package<sup>[36]</sup> into terms as shown in Equation (1):

$$\Delta E = \Delta E_{\text{FRZ}} + \Delta E_{\text{POL}} + \Delta E_{\text{CT}} \quad (1)$$

The frozen (FRZ) term is defined as the change in energy from bringing together two fragments that are far apart without allowing any molecular orbital (MO) relaxation and can be further broken down into electrostatics (ELEC), Pauli repulsion (PAULI), and dispersion (DISP) energies (Eq (2)):

$$\Delta E_{\text{FRZ}} = (\Delta E_{\text{ELEC}} + \Delta E_{\text{PAULI}}) + \Delta E_{\text{DISP}} \quad (2)$$

The polarization term is described as the intrafragment relaxation of the frozen occupied MOs of each fragment. The charge transfer (CT) term is derived from further interfragment relaxation of the frozen occupied MOs of each fragment.

In assessing the values of the ALMO-EDA terms, initial focus was placed on evaluating the frozen terms because these do not include fragment relaxation and encompass electrostatic effects. Table 4 shows that both IPFB and IDNB/acceptor complexes have comparable electrostatic/Pauli repulsion (computed as a combined ELEC + PAULI) terms for a given acceptor and are repulsive overall. The greater repulsion observed with better acceptors is consistent with their closer interactions

**Table 4.** Deconvoluted frozen (FRZ) term ( $\Delta E_{\text{FRZ}} = (\Delta E_{\text{ELEC}} + \Delta E_{\text{PAULI}}) + \Delta E_{\text{DISP}}$ ) in kcal mol<sup>-1</sup> as dispersion (DISP), electrostatics (ELEC), and Pauli repulsion (PAULI) energies in ALMO-EDA for IPFB/acceptor complexes and IDNB/acceptor complexes

XB Donor/Acceptor Complex	ELEC + PAULI	DISP	$\Delta E_{\text{FRZ}}$
IPFB/3-NPy	0.69	-0.83	-0.14
IPFB/3-FPy	1.21	-1.00	0.21
IPFB/PY	2.11	-1.19	0.92
IPFB/DMAP	3.32	-1.46	1.86
IDNB/3-NPy	1.09	-0.76	0.33
IDNB/3-FPy	1.06	-0.86	0.20
IDNB/PY	1.51	-1.00	0.51
IDNB/DMAP	2.64	-1.28	1.36

**Table 5.** Summary of interaction energies ( $\Delta E = \Delta E_{\text{FRZ}} + \Delta E_{\text{POL}} + \Delta E_{\text{CT}}$ ) in kcal mol<sup>-1</sup> deconvoluted into 3 energy terms (frozen (FRZ), polarization (POL), and charge transfer (CT)) in ALMO-EDA for IPFB/acceptor complexes and IDNB/acceptor complexes.

XB Donor/Acceptor Complex	FRZ	POL	CT	$\Delta E$
IPFB/3-NPy	-0.14	-1.06	-4.06	-5.26
IPFB/3-FPy	0.21	-1.51	-4.97	-6.27
IPFB/PY	0.92	-2.02	-6.02	-7.12
IPFB/DMAP	1.86	-3.13	-7.84	-9.11
IDNB/3-NPy	0.33	-0.98	-3.67	-4.32
IDNB/3-FPy	0.20	-1.32	-4.31	-5.43
IDNB/PY	0.51	-1.68	-5.05	-6.22
IDNB/DMAP	1.36	-2.69	-6.66	-7.99

(Table S4 in Supporting Information) and a dominance of the Pauli repulsion term. The dispersion terms in IPFB and IDNB/acceptor complexes are very similar to one another and are attractive (negative values) for a given acceptor.

Including intrafragment (polarization) and interfragment (charge transfer) relaxation in the ALMO-EDA results gives the full picture of the energy terms influencing halogen bonding strength (Table 5, Table S5 in Supporting Information for Cartesian coordinates). IPFB/acceptor complexes show a significantly larger charge transfer contribution, relative to the total interaction energy, than IDNB/acceptor complexes which counter the trends from the frozen terms. This finding echoes the results on iodomethane derivatives.<sup>[37]</sup> The implication of larger CT in IPFB than IDNB/acceptor complexes, which is reflected in the theoretical binding energies, is indicative of greater dimer stabilization (C—I...N), more so in IPFB/acceptor complexes than IDNB/acceptor complexes. The polarization terms, while not as prominent as CT in either IPFB or IDNB/acceptor complexes, are also attractive in nature and contribute to complex stability.

### Observation of halogen bonding in solution

While general agreement is found between the gas phase  $\Delta E_{\text{bind}}$  and  $\Delta V_s$  for halogen bonding predictions, the discrepancy in ordering the relative binding strengths of XB donor/acceptor complexes featuring XB donors with fluoro and nitro substituents, motivated comparison to experimental results for halogen bonding interactions. All XB donor and acceptor pairs were analyzed via Raman spectroscopy in order to assess halogen bonding interaction trends between and perturbations within the molecules. Raman spectroscopy was employed for analysis of halogen bonding in solution studies due to detection sensitivity toward the formation of halogen bonded complexes. Red shifted C—I vibrational frequencies ( $\nu$ ) of XB donors, denoting XB complex formation, were analyzed. The compilation of C—I stretching frequencies are shown for each XB donor and complex (if detected) in Table 6.

For each Raman experiment, the C—I stretching vibrational frequencies of unbound 1.00 mol/kg (molal) solutions of the XB donors (except 0.220 mol/kg p-NIB due to limited solubility)

**Table 6.** C—I stretching vibrational frequency ( $\nu$ ) in cm<sup>-1</sup> of each unbound XB donor and each complex observed in CH<sub>2</sub>Cl<sub>2</sub>.

XB Donors and XB Complexes	C—I Raman Shift (cm <sup>-1</sup> )
IB	266.0
p-NIB	213.6
DFIB	218.7
DFIB/DMAP	211.7 <sup>[a]</sup>
IPFB	204.0
IPFB/3-FPy	197.2 <sup>[a]</sup>
IPFB/PY	194.6 <sup>[a]</sup>
IPFB/DMAP	190.0 <sup>[a]</sup>
IDNB	241.9
IDNB/DMAP	233.4 <sup>[a]</sup>

[a] Red shifted peaks of formed complexes.



were examined as reference points to evaluate the magnitude of potential red shifting in C–I stretches due to interactions with XB acceptors. Upon the addition of the XB acceptors (0.500 equiv, 1.00 equiv, and 1.50 equiv), the extent to which halogen bonding interactions were taking place, through the observation of newly formed, red shifted C–I peaks signifying complexation (iodine interacting with pyridyl nitrogen: C–I...N), was evaluated. Raman spectra for IB, p-NIB, and DFIB/acceptor mixtures were predicted to form weak XB donor/acceptor interactions by both computed  $\Delta V_s$  and  $\Delta E_{\text{bind}}$ . The XB donor/acceptor mixtures contained only the C–I stretching vibrational frequency of unbound IB at  $\nu=266.0\text{ cm}^{-1}$ , unbound p-NIB at  $\nu=213.6\text{ cm}^{-1}$ , and unbound DFIB at  $\nu=218.7\text{ cm}^{-1}$  (with the exception of DFIB/DMAP mixtures shown in Figure S1 in Supporting Information).

In contrast to a purely electrostatic model based on  $\Delta V_s$ ,  $\Delta E_{\text{bind}}$  predicts that IPFB binds more strongly with XB acceptors than IDNB. Interactions between IPFB/acceptors (3-NPy, 3-FPy, PY, and DMAP) were evaluated and the following observed: complex formation, denoted by a red shift in newly formed C–I peak compared to that of unbound IPFB at  $\nu=190.0\text{ cm}^{-1}$ , was observed in all XB acceptor concentrations except with 3-NPy (the weakest Lewis base). Figure 4a with IPFB/3-FPy mixtures illustrates the presence of the C–I...N interaction from new, red shifted C–I vibrational stretching frequency at  $\nu=197.2\text{ cm}^{-1}$ , which is consistent with the  $\Delta E_{\text{bind}}$  predictions for the IPFB/3-FPy complexes. IPFB/PY complexes with C–I stretches at  $\nu=194.6\text{ cm}^{-1}$  (Figure 4b) and IPFB/DMAP complexes with C–I stretches at  $\nu=190.0\text{ cm}^{-1}$  (Figure 4c) show distinct peak formation consistent with stronger halogen bonding interactions than 3-FPy complexes. The more intense red shifted peak formation within IPFB/DMAP complexes was found as the molar ratio of DMAP increased. This correlates back to the strength of

DMAP as a good XB acceptor from the predictions of both  $\Delta E_{\text{bind}}$  and  $\Delta V_s$  computed calculations.

The experimental outcome of the interactions between IDNB/acceptors was not predicted by the ESPs. IDNB, in comparison to the other XB donors, has the largest  $\sigma$ -hole region and  $V_{s,\text{max}}$  value which suggests the most favorable interactions to occur with the addition of a XB acceptor (large computed  $\Delta V_s$ ). Therefore, the formation of new red-shifted C–I stretches were expected to be observed in all IDNB/acceptor solution experiments. However, analysis of the Raman spectra yielded only one successful complexation experiment (IDNB/DMAP) with a red shifted peak at  $\nu=233.4\text{ cm}^{-1}$  (Figure 5) and  $241.9\text{ cm}^{-1}$  for unbound IDNB.

Raman spectra of IPFB/acceptor complexes and IDNB/acceptor complexes were compared to resolve which predictions (i.e.  $\Delta E_{\text{bind}}$  or  $\Delta V_s$ ) more accurately suggest the orders and strengths of halogen bonding propensities. Note,  $\Delta E_{\text{bind}}$  are directly related to the observed red shifts in the Raman spectra (Figure S2 in Supporting Information), where the relationship between the two is as follows: with strong binding affinity there is also a large shift in the C–I stretch from the unbound to the bound halogen bond donor. Raman spectra reveal  $\Delta E_{\text{bind}}$  does reflect the distinct interaction strength hierarchy between IPFB/acceptor complexes and IDNB/acceptor complexes exhibited in the Raman spectra. Notably, the computed C–I...N interaction distances in IPFB and IDNB/acceptor complexes are consistent with the theoretical binding energy predictions (see Figure S4 in Supporting Information) rather than ESP predictions. Additionally, relative areas of the bound and unbound states were used to estimate  $\Delta G$  values for the observed complexes (see Table S6 in Supporting Information). The relative concentration of the bound states for each observed complex was found to increase with increasing acceptor strengths ( $\Delta G$  values become more negative) across a particular XB donor/acceptor complex.

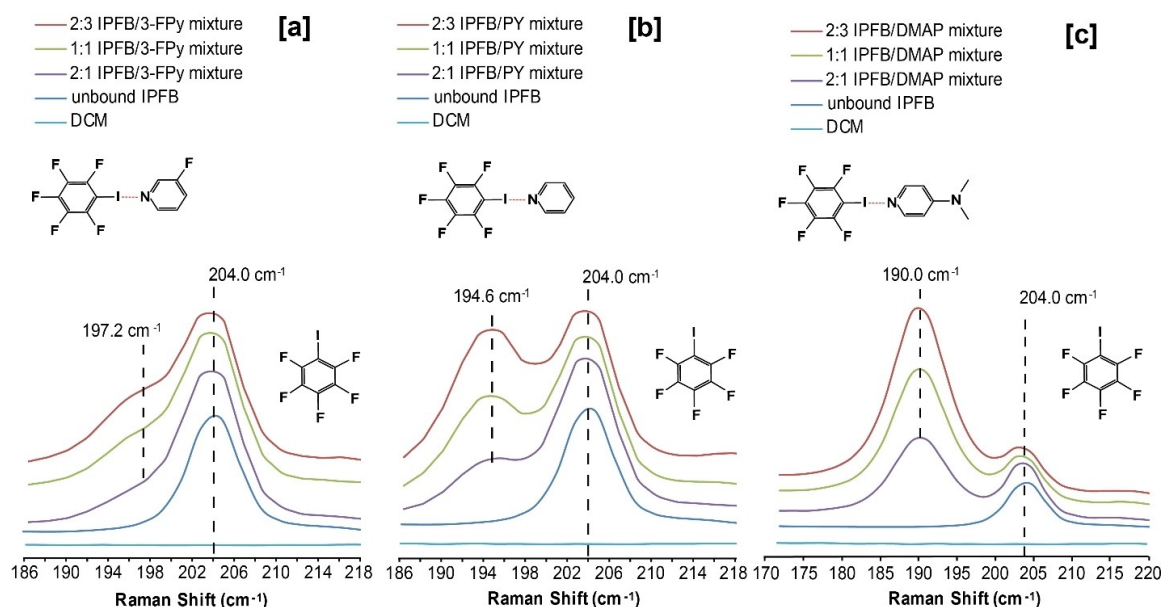
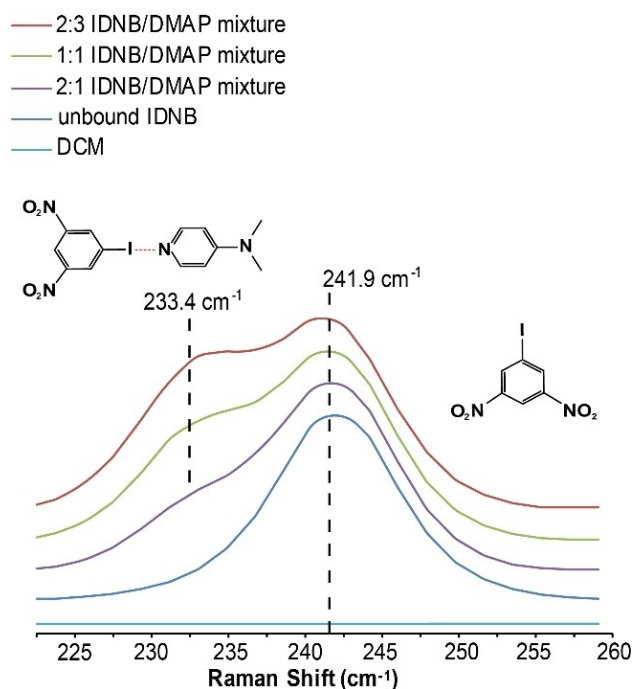


Figure 4. a–c. Raman spectra of unbound IPFB and 2:3, 1:1, and 2:1 molar ratios of a. IPFB/3-FPy solutions, b. IPFB/PY, and c. IPFB/DMAP solutions.



**Figure 5.** Raman spectra of unbound IDNB and 2:3, 1:1, and 2:1 molar ratios of IDNB/DMAP solutions.

Overall, IPFB is proven, experimentally and in agreement with  $\Delta E_{\text{bind}}$  predictions, to be the stronger interacting XB donor despite having a somewhat smaller  $\sigma$ -hole magnitude than IDNB. The origin of this is contributed to a greater degree of CT within IPFB/acceptor complexes than IDNB/acceptor complexes.

## Conclusion

The most common method for predicting halogen bonding propensities, electrostatic potential calculations, fails to reproduce theoretical or experimental binding properties for highly activated halogen bond donors. Raman spectroscopy was employed to observe both the extent of C–I vibrational frequency shifts in solution of XB donor when a XB acceptor solution was added and to evaluate the population of the bound state relative to the ranking of interaction strengths. These studies unambiguously demonstrate that a model based on the electrostatics of the uncomplexed donor has limited predictive ability even in a relative sense. IPFB and IDNB/complexes containing the most powerful acceptors were further evaluated using ALMO-EDA revealing that, although larger  $\sigma$ -holes are generally indicative of stronger binding affinity, partitioning into charge transfer, frozen, and polarization terms points to significant charge transfer interactions in differentiating binding strength. The findings inform broad applications in the fields of chemistry, crystal engineering, and molecular recognition because reliable methods to predict strong non-covalent interactions in solid, solution, and gas phases are essential for populating the supramolecular design toolbox.

## Experimental Section

### General

Density functional theory (DFT) and electrostatic potential maps (mapped on 0.002 e/au electron density contour) were calculated at the B3LYP level of theory and 6-311G\*\* basis set with Spartan '16 software (Wavefunction Inc., Irvine, CA). Energies in the gas phase (B3LYP-D3/6-311G\*\*) and solution phase with the Conductor like Polarizable Continuum Model (C-PCM) in DCM (dielectric constant=8.93) at B3LYP/6-311G\*\* were calculated with Spartan '18 software. Starting geometrics were set to mimic halogen bonding interactions found in the CSD (Cambridge Structural Database), where all interactions were built to interact at a  $\sim 180^\circ$  bond angle for C–I...N interactions with energy minimization. The achievement of minimum energy geometry was confirmed by the absence of imaginary frequencies. Single point energy and second generation ALMO-EDA calculations were performed at the B3LYP/6-311G\*\* level of theory using the Q-Chem 5.3.2 software package for iodopentafluorobenzene and 1-iodo-3,5-dinitrobenzene/acceptor complexes. All reagents were commercially available, purchased, and used without any additional purification. Raman spectra were recorded at room temperature using a Renishaw inVia Qontor Raman Microscope (Laser  $\lambda = 532$  nm) featuring a Leica microscope, 1800 lines/mm gratings, a CCD area detector, and 50  $\mu\text{m}$  slit size. Using WiRE 3.4 software package (Renishaw) and a silicon internal standard for calibration, spectra for the XB solution experiments were collected via 50 increments of scans at 0.5 secs per scan in static mode, with a range of 120–820 reciprocal wavelength ( $\text{cm}^{-1}$ ). The chemical shifts are given in  $\text{cm}^{-1}$ , the signal of the dissolved halogen bond donors' C–I vibrational frequency shifts (at  $\nu = 190$ – $266$   $\text{cm}^{-1}$ ) have been used as reference signals.

### Experimental Setup

Stock solutions of 5.00 mL of 1.00 mol/kg XB donors ( $\sim 0.220$  mol/kg p-NIB due to low solubility) were made, in dry solvent DCM, in tared 20 mL vials by converting the molecular weight ( $\text{g mol}^{-1}$ ) of each XB donor to moles (mol) then dividing it by kilograms (kg) of solvent DCM. DCM was selected as the solvent for Raman solution studies because it dissolves the XB donors and acceptors without contributing peaks that overlap with those of interest in the XB donor/acceptor complexes. The XB acceptor stock solution concentrations were made from the serial dilution of 5.00 mL of 1.50 mol/kg. Solutions at 1.00 mol/kg were achieved by aliquoting 1.90 mL of the 1.50 mol/kg stock solution into a 10 mL graduated cylinder and diluting it with DCM to a final volume of 3.00 mL then pipetted into a 4 mL vial. Solutions at 0.500 mol/kg were achieved by aliquoting 1.00 mL of the 1.00 mol/kg stock solution into a graduated cylinder and diluting it with DCM to a final volume of 2.00 mL then pipetted into a 4 mL vial. Each donor solution (200  $\mu\text{L}$ ) and acceptor solution (200  $\mu\text{L}$ ), 1:1 by volume, were added to a clean 4 mL vial then placed on the stage of the Raman microscope and data collected with a 5 $\times$  objective lens.

### Acknowledgements

The authors acknowledge Dr. Ren Wiscons for providing technical support and useful discussions. This work was supported by the Army Research Office (ARO) in the form of a MURI (W911NF-13-1-0387). The authors also gratefully acknowledge Rackham Graduate School for the Rackham Graduate Student Research Grant for financial support.

## Conflict of Interest

The authors declare no conflict of interest.

**Keywords:** density functional calculations · halogen bonding · noncovalent interactions · Raman spectroscopy · solution phase

- [1] R. Wilcken, M. O. Zimmermann, A. Lange, A. C. Joerger, F. M. Boeckler, *J. Med. Chem.* **2013**, *56*, 1363–1388.
- [2] T. M. Beale, M. G. Chudzinski, M. G. Sarwar, M. S. Taylor, *Chem. Soc. Rev.* **2013**, *42*, 1667–1680.
- [3] J. Heidrich, T. E. Exner, F. M. Boeckler, *J. Chem. Inf. Model.* **2019**, *59*, 636–643.
- [4] P. Metrangolo, F. Meyer, T. Pilati, G. Resnati, G. Terraneo, *Angew. Chem. Int. Ed.* **2008**, *47*, 6114–6127; *Angew. Chem.* **2008**, *120*, 6206–6220.
- [5] M. Erdélyi, *Chem. Soc. Rev.* **2012**, *41*, 3547–3557.
- [6] T. Clark, M. Hennemann, J. S. Murray, P. Politzer, *J. Mol. Model.* **2007**, *13*, 291–296.
- [7] P. Politzer, J. S. Murray, T. Clark, *Phys. Chem. Chem. Phys.* **2010**, *12*, 7748–7757.
- [8] G. Cavallo, P. Metrangolo, R. Milani, T. Pilati, A. Priimagi, G. Resnati, G. Terraneo, *Chem. Rev.* **2016**, *116*, 2478–2601.
- [9] P. Politzer, J. S. Murray, T. Clark, *Phys. Chem. Chem. Phys.* **2013**, *15*, 11178–11189.
- [10] J. S. Murray, P. Lane, P. Politzer, *J. Mol. Model.* **2009**, *15*, 723–729.
- [11] H. Fan, J. K. Eliason, C. D. Moliva A., J. L. Olson, S. M. Flancher, M. W. Gealy, D. J. Ulness, *J. Phys. Chem. A* **2009**, *113*, 14052–14059.
- [12] B. Hawthorne, H. Fan-Hagenstein, E. Wood, J. Smith, T. Hanks, *Int. J. Spectrosc.* **2013**, *2013*, 1–10.
- [13] C. Präsang, A. C. Whitwood, D. W. Bruce, *Cryst. Growth Des.* **2009**, *9*, 5319–5326.
- [14] A. Siiskonen, A. Priimagi, *J. Mol. Model.* **2017**, *23*, 50.
- [15] L. P. Wolters, P. Schyman, M. J. Pavan, W. L. Jorgensen, F. M. Bickelhaupt, S. Kozuch, *Wiley Interdiscip. Rev.: Comput. Mol. Sci.* **2014**, *4*, 523–540.
- [16] D. Musumeci, C. A. Hunter, R. Prohens, S. Scuderi, J. F. McCabe, *Chem. Sci.* **2011**, *2*, 883–890.
- [17] J. S. Murray, P. Politzer, *Wiley Interdiscip. Rev.: Comput. Mol. Sci.* **2011**, *1*, 153–163.
- [18] J. S. Murray, P. Politzer, *J. Mol. Struct.: THEOCHEM* **1998**, *425*, 107–114.
- [19] K. B. Landenberger, A. J. Matzger, *Cryst. Growth Des.* **2010**, *10*, 5341–5347.
- [20] P. Politzer, J. S. Murray, T. Clark, G. Resnati, *Phys. Chem. Chem. Phys.* **2017**, *19*, 32166–32178.
- [21] N. R. Goud, O. Bolton, E. C. Burgess, A. J. Matzger, *Cryst. Growth Des.* **2016**, *16*, 1765–1771.
- [22] M. D. Perera, J. Desper, A. S. Sinha, C. B. Aakeröy, *CrystEngComm* **2016**, *18*, 8631–8636.
- [23] C. A. Gunawardana, C. B. Aakeröy, *Chem. Commun.* **2018**, *54*, 14047–14060.
- [24] A. Bauzá, D. Quiñonero, A. Frontera, P. M. Deyá, *Phys. Chem. Chem. Phys.* **2011**, *13*, 20371–20379.
- [25] R. A. Wiscons, V. Coropceanu, A. J. Matzger, *Chem. Mater.* **2019**, *31*, 6598–6604.
- [26] J. Yang, B. Hong, N. Wang, X. Li, X. Huang, Y. Bao, C. Xie, H. Hao, *CrystEngComm* **2019**, *21*, 6374–6381.
- [27] C. B. Aakeröy, T. K. Wijethunga, J. Desper, *J. Mol. Struct.* **2014**, *1072*, 20–27.
- [28] B. A. DeHaven, A. L. Chen, E. A. Shimizu, S. R. Salpage, M. D. Smith, L. S. Shimizu, *Cryst. Growth Des.* **2019**, *19*, 5776–5783.
- [29] C. B. Aakeröy, T. K. Wijethunga, J. Desper, M. Đaković, *Cryst. Growth Des.* **2016**, *16*, 2662–2670.
- [30] C. B. Aakeröy, P. D. Chopade, J. Desper, *Cryst. Growth Des.* **2013**, *13*, 4145–4150.
- [31] T. Clark, *WIREs Comput. Mol. Sci.* **2013**, *3*, 13–20.
- [32] G. R. Desiraju, P. S. Ho, L. Kloo, A. C. Legon, R. Marquardt, P. Metrangolo, P. Politzer, G. Resnati, K. Rissanen, *Pure Appl. Chem.* **2013**, *85*, 1711–1713.
- [33] A. J. Stone, *J. Am. Chem. Soc.* **2013**, *135*, 7005–7009.
- [34] S. Kozuch, J. M. L. Martin, *J. Chem. Theory Comput.* **2013**, *9*, 1918–1931.
- [35] Y. Lu, H. Li, X. Zhu, H. Liu, W. Zhu, *Int. J. Quantum Chem.* **2012**, *112*, 1421–1430.
- [36] Y. Shao, Z. Gan, E. Epifanovsky, A. T. B. Gilbert, M. Wormit, J. Kussmann, A. W. Lange, A. Behn, J. Deng, X. Feng, D. Ghosh, M. Goldey, P. R. Horn, L. D. Jacobson, I. Kaliman, R. Z. Khaliullin, T. Kuš, A. Landau, J. Liu, E. I. Proynov, Y. M. Rhee, R. M. Richard, M. A. Rohrdanz, R. P. Steele, E. J. Sundstrom, H. L. Woodcock III, P. M. Zimmerman, D. Zuev, B. Albrecht, E. Alguire, B. Austin, G. J. O. Beran, Y. A. Bernard, E. Berquist, K. Brandhorst, K. B. Bravaya, S. T. Brown, D. Casanova, C.-M. Chang, Y. Chen, S. H. Chien, K. D. Closser, D. L. Crittenden, M. Diederhofen, R. A. D. Jr, H. Do, A. D. Dutoi, R. G. Edgar, S. Fatehi, L. Fusti-Molnar, A. Ghysels, A. Golubeva-Zadorozhnaya, J. Gomes, M. W. D. Hanson-Heine, P. H. P. Harbach, A. W. Hauser, E. G. Hohenstein, Z. C. Holden, T.-C. Jagau, H. Ji, B. Kaduk, K. Khistyayev, J. Kim, J. Kim, R. A. King, P. Klunzinger, D. Kosenkov, T. Kowalczyk, C. M. Krauter, K. U. Lao, A. D. Laurent, K. V. Lawler, S. V. Levchenko, C. Y. Lin, F. Liu, E. Livshits, R. C. Lochan, A. Luenser, P. Manohar, S. F. Manzer, S.-P. Mao, N. Mardirossian, A. V. Marenich, S. A. Maurer, N. J. Mayhall, E. Neuscamman, C. M. Oana, R. Olivares-Amaya, D. P. O'Neill, J. A. Parkhill, T. M. Perrine, R. Peverati, A. Prociuk, D. R. Rehn, E. Rosta, N. J. Russ, S. M. Sharada, S. Sharma, D. W. Small, A. Sodt, T. Stein, D. Stück, Y.-C. Su, A. J. W. Thom, T. Tsuchimochi, V. Vanovschi, L. Vogt, O. Vydrov, T. Wang, M. A. Watson, J. Wenzel, A. White, C. F. Williams, J. Yang, S. Yeganeh, S. R. Yost, Z.-Q. You, I. Y. Zhang, X. Zhang, Y. Zhao, B. R. Brooks, G. K. L. Chan, D. M. Chipman, C. J. Cramer, W. A. Goddard III, M. S. Gordon, W. J. Hehre, A. Klamt, H. F. Schaefer III, M. W. Schmidt, C. D. Sherrill, D. G. Truhlar, A. Warshel, X. Xu, A. Aspuru-Guzik, R. Baer, A. T. Bell, N. A. Besley, J.-D. Chai, A. Dreuw, B. D. Dunietz, T. R. Furlani, S. R. Gwaltney, C.-P. Hsu, Y. Jung, J. Kong, D. S. Lambrecht, W. Liang, C. Ochsenfeld, V. A. Rassolov, L. V. Slipchenko, J. E. Subotnik, T. V. Voorhis, J. M. Herbert, A. I. Krylov, P. M. W. Gill, M. Head-Gordon, *Mol. Phys.* **2015**, *113*, 184–215.
- [37] J. Thirman, E. Engelage, S. M. Huber, M. Head-Gordon, *Phys. Chem. Chem. Phys.* **2018**, *20*, 905–915.

Manuscript received: July 12, 2021

Accepted manuscript online: September 21, 2021

Version of record online: October 6, 2021